Check for updates

AGU ADVANCING EARTH AND SPACE SCIENCE

Geophysical Research Letters®

RESEARCH LETTER
10.1029/2022GL099488

The Role of Extratropical Pacific in Crossing ENSO Spring Predictability Barrier

Yingying Zhao[1], Yishuai Jin[2], Jianping Li[3], and Antonietta Capotondi[4,5]

[1]Deep-sea Research Center, Pilot National Laboratory for Marine Science and Technology (Qingdao), Qingdao, China, [2]Frontier Science Center for Deep Ocean Multispheres and Earth System (FDOMES) and Physical Oceanography Laboratory, Ocean University of China, Qingdao, China, [3]Frontier Science Center for Deep Ocean Multispheres and Earth System (FDOMES) and Physical Oceanography Laboratory and Academy of the Future Ocean, Ocean University of China, Qingdao, China, [4]Cooperative Institute for Research in Environmental Sciences, University of Colorado, Boulder, CO, USA, [5]Physical Sciences Laboratory, NOAA, Boulder, CO, USA

Abstract This paper investigates the impacts of extratropical Pacific on El Niño-Southern Oscillation (ENSO) spring predictability barrier (SPB). Using an empirical dynamical model – Linear Inverse Model (LIM), we find that the dynamics of the northern and southern extratropical Pacific can significantly and equally weaken the Eastern Pacific (EP)-ENSO SPB, while the North Pacific is more important for weakening the Central Pacific (CP)-ENSO SPB. The evolution of the extratropical optimum initial structures illustrates the different roles of the northern and southern extratropical Pacific in crossing EP and CP ENSO SPBs and demonstrates the decisive role that the South Pacific initial condition plays in ENSO diversity. Additionally, the extratropical Pacific greatly influences the forecast skill of El Niño during SPB, while tropical dynamics may be more important for crossing the SPB of La Niña.

Plain Language Summary The spring predictability barrier (SPB) is a sudden reduction of the prediction skill of the El Niño-Southern Oscillation (ENSO) in the boreal spring. Using a linear dynamical model, we find the correlation forecast skill of Central Pacific ENSO in boreal spring and summer is significantly enhanced by including the dynamics of northern extratropical Pacific, therefore weakening the SPB. For the Eastern Pacific ENSO, both the northern and southern extratropical dynamics are equally important for weakening the SPB. Our results also show that the initial state of southern extratropical Pacific may determine the type of ENSO. Additionally, including the extratropical dynamics helps to improve the forecast skill of El Niño events in boreal spring and summer while the extratropical dynamics may not be essential for the prediction of La Niña.

Key Points:

- A linear dynamical model suggests that including the dynamics of extratropical Pacific can significantly weaken the ENSO SPB
- North Pacific plays a role both in the central and eastern Pacific, while South Pacific may be essential in determing ENSO diversity
- Extratropical Pacific greatly influences the forecast skill of El Niño during SPB, while the impact on La Niña is limited

Supporting Information:

Supporting Information may be found in the online version of this article.

Correspondence to:

Y. Jin,
jinyishuai@126.com

Citation:

Zhao, Y., Jin, Y., Li, J., & Capotondi, A. (2022). The role of extratropical Pacific in crossing ENSO spring predictability barrier. *Geophysical Research Letters*, *49*, e2022GL099488. https://doi.org/10.1029/2022GL099488

Received 9 MAY 2022
Accepted 3 AUG 2022

© 2022. American Geophysical Union. All Rights Reserved.

1. Introduction

The El Niño-Southern Oscillation (ENSO) is the dominant interannual variability in the tropical Pacific, showing impacts on weather and climate worldwide through atmospheric teleconnections (Alexander et al., 2002; Capotondi et al., 2020; Deser et al., 2012; Di Lorenzo et al., 2010; Liu & Di Lorenzo, 2018). Thus, accurate simulation and prediction of ENSO one or more seasons in advance is of great importance. However, one significant obstacle in ENSO prediction is the spring predictability barrier (SPB), which consists of a dramatic drop in forecast skill when the prediction is made through spring (Z. Hou et al., 2018; Jin et al., 2008, 2019, 2020; Webster & Yang, 1992; Wu et al., 2009; Xue et al., 1994). One possible reason that leads to this SPB is the specific initial errors in the tropical Pacific (Mu, Duan, & Wang, 2007, 2007b). However, recent studies have identified numerically and analytically that the seasonally varying background of the tropical Pacific may be an important factor in causing the SPB (Y. Jin et al., 2019, 2020, 2021; Y. Jin and Liu, 2021a, b; A. F. Levine and McPhaden, 2015; Liu et al., 2019).

The role of the extratropical Pacific in energizing ENSO has been studied extensively. Through observations and coupled general circulation models, D. J. Vimont et al. (2001, 2003a, 2003b) proposed a seasonal footprinting mechanism, that is, the tropical atmosphere is forced during spring and summer by sea surface temperature (SST) anomalies generated by midlatitude atmospheric variability during the previous winter. Meanwhile, North and South Pacific meridional modes (NPMM and SPMM) have been identified to play important roles in inducing ENSO events (Chang et al., 2007; Ding, Li, Tseng, Sun, & Guo, 2015, b; H. Zhang et al., 2014). As ENSO exhibits different

spatial patterns, usually classified in terms of Eastern-Pacific (EP) and Central-Pacific (CP) types (i.e., ENSO diversity; Capotondi et al., 2015; Capotondi et al., 2021), recent studies suggested that the North Pacific Oscillation (NPO) or NPMM is more important to the development of CP-ENSO (Yu & Kim, 2011), while the South Pacific Oscillation (SPO) or SPMM is more related to EP-ENSO (You & Furtado, 2018; H. Zhang et al., 2014). In addition to ENSO diversity, ENSO asymmetries between El Niño and La Niña may also be influenced by the extratropical Pacific. Anderson, Furtado, et al. (2013) found that boreal winter near-surface atmospheric circulations over the Hawaiian region have an additional influence on the longitudinal position of the resultant ENSO-related SST, with warm (cold) events systematically shifted to the east (west) of the typical SST anomalies.

Since the extratropical Pacific plays an important role in triggering ENSO, it may also have potential impacts on ENSO predictability. According to this hypothesis, through the linear regression methodologies, Pegion et al. (2020) found that at a 1-year lead time, the extratropical Pacific is responsible for the formation of CP-ENSO, but not EP-ENSO. Chen et al. (2020) found that by combining tropical preconditions with extratropical precursors, ENSO prediction skill could be noticeably increased beyond the time scale of the SPB. Tseng et al. (2022) indicated that the predictability of CP-ENSO (EP-ENSO) could be significantly improved by including northern (southern) extratropical precursors on a "tropical predictors only" linear regression forecast model. However, to our knowledge, the effect of the extratropical Pacific on SPB, especially on the two types of ENSO SPB and El Niño/La Niña SPB, is less studied.

Linear Inverse Models (LIMs) have been successfully used to capture features of observed seasonal tropical SST variability and predictability (e.g., Penland & Matrosova, 1994; Penland & Sardeshmukh, 1995 (hereafter PS95); Newman, 2007; Newman et al., 2011). Zhao et al. (2021) explored the impacts of tropical dynamics on the North Pacific climate variability by decoupling the tropical Pacific and North Pacific through the LIM. In this study, we extend Zhao et al. (2021)'s analysis by building a 3-state LIM, which incorporates monthly anomalies of SST and sea surface height (SSH) of North Pacific, tropical Pacific, and South Pacific, to study the impact of the extratropical Pacific on the ENSO SPB.

2. Data and Method

2.1. Observation Data and ENSO Indices

The data used in this study includes monthly mean values of SST (unit: °C) and SSH (unit: m) from the European Center for Medium-Range Weather Forecasting (ECMWF) Ocean Reanalysis System 4 (ORAS4) (Balmaseda et al., 2013). SST and SSH fields from January 1958 to December 2015 are first averaged into 2° latitude × 5° longitude grid boxes and then the climatological seasonal cycle is removed. 10-m wind components (U and V) from the National Centers for Environmental Prediction (NCEP) Reanalysis (Kalnay et al., 1996) are also used, which are represented at a 1.875-° (∼1.9-°) resolution in the meridional (zonal) direction. The wind stress anomalies are derived by removing the mean seasonal cycle and a long-term linear trend.

For simplicity, the typical Niño3 and Niño4 indices are used to represent the EP-ENSO and CP-ENSO (M. Hou et al., 2019). Note that using other indices (N_{EP} and N_{CP} indices defined by H. L. Ren and Jin (2011), see supplemental material Text S2 and Figure S6 in Supporting Information S1) to represent ENSO diversity do not qualitatively change the results. Niño3 and Niño4 indices are calculated as SST anomalies averaged over the Niño3 (5°S–5°N, 150°W–90°W) and Niño4 (5°S–5°N, 160°E−150°W) regions, respectively. The Niño3.4 index, defined as the SST anomalies averaged over the Niño3.4 region (5°S–5°N, 170°W–120°W), is also used to investigate the impact of extratropical Pacific on the predictability of different phases of ENSO events (i.e., El Niño and La Niña). El Niño (La Niña) years are defined when the seasonal Niño 3.4 index during November, December, and the following January (NDJ) is larger (smaller) than 1 (−1) °C(Figure S1, see Text S3 in Supporting Information S1 for the specific years).

2.2. Build the LIM

In the LIM framework, the evolution of a dynamical system is represented following PS95 as:

$$\frac{d\mathbf{x}}{dt} = \boldsymbol{L}\mathbf{x} + \xi, \tag{2.1}$$

where x is the anomalous climate state vector; L is the linear dynamical evolution operator; ξ is the white noise forcing. L can be determined based on the covariance of the state vector x, as described in PS95:

$$\boldsymbol{L} = \tau_0^{-1} ln \left\{ \boldsymbol{C}\left(\tau_0\right) \boldsymbol{C}(0)^{-1} \right\}, \tag{2.2}$$

where $\boldsymbol{C}(0) = x(t)x^T(t)$ and $\boldsymbol{C}\left(\tau_0\right) = x\left(t+\tau_0\right)x^T(t)$ represent the covariance matrix and lag-covariance matrix at lag τ_0, respectively. In this work, we choose $\tau_0 = 1$ month. The fluctuation-dissipation relation determines the spatial statistics of the white noise forcing:

$$\boldsymbol{L}\boldsymbol{C}(0) + \boldsymbol{C}(0)\boldsymbol{L}^T + \boldsymbol{Q} = 0, \tag{2.3}$$

where the noise covariance matrix $\boldsymbol{Q} = \xi\xi^T dt$.

To reduce the number of spatial degrees of freedom, Empirical Orthogonal Function (EOF) analysis is applied to the monthly SST and SSH fields, respectively. SST and SSH variabilities have different overall magnitudes, which may influence the results. To avoid the possible impacts of different magnitudes, each field is normalized by its domain-averaged climatological standard deviation before computing the EOFs. Following the approach of Frankignoul et al. (2017) and Zhao et al. (2021), the projection on the least damped stationary eigenmode from a LIM, which includes SST and SSH anomalies covering the entire Pacific basin (90°S–90°N), is subtracted from the original data to remove the externally forced trend. The resulting "detrended" SST and SSH data then form the basis for the following analysis. Note that using different methods to remove the trend does not qualitatively change the results.

To investigate the dynamics of the coupled tropical/extra-tropical Pacific system, we use the following state vector:

$$\mathrm{x} = \begin{bmatrix} SST_T \\ SSH_T \\ SST_N \\ SSH_N \\ SST_S \\ SSH_S \end{bmatrix}, \tag{2.4}$$

where the subscripts T, N, and S represent the variables within the tropical Pacific (TP) (10°S − 10°N), North Pacific (NP) (14°N − 60°N), and South Pacific (SP) (60°S − 14°S), respectively. The state vector x is then constructed based on the corresponding PC time series of SST and SSH anomalies in these Pacific regions. After doing the truncation test 1 (see Text S1 and Figure S2 in Supporting Information S1), we incorporate 12/4/6/4/6/4 leading PCs of SST_T/ SSH_T/ SST_N/ SSH_N/ SST_S/ SSH_S in the state vector of the LIM (hereafter Full LIM), which explains about 92/77/52/38/52/44% of the variability of their respective fields.

To confirm the validity of the Full LIM, we compare the predicted lag-covariability of LIM, $\boldsymbol{C}(\tau) = exp(\boldsymbol{L}\tau)\boldsymbol{C}(0)$, to the observation for lags greater than the training lag (Figure S3 in Supporting Information S1), and find that the Full LIM can capture all salient aspects of the observed SST lag-covariance pattern.

2.3. Using the LIM to Decouple Tropical Pacific and Extratropical Pacific

With the state vector x of Full LIM in Equation 2.3, Equation 2.1 can be rewritten as:

$$\frac{dx}{dt} = \frac{d}{dt}\begin{bmatrix} x_T \\ x_N \\ x_S \end{bmatrix} = \begin{bmatrix} \boldsymbol{L_{TT}}\ \boldsymbol{L_{NT}}\ \boldsymbol{L_{ST}} \\ \boldsymbol{L_{TN}}\ \boldsymbol{L_{NN}}\ \boldsymbol{L_{SN}} \\ \boldsymbol{L_{TS}}\ \boldsymbol{L_{NS}}\ \boldsymbol{L_{SS}} \end{bmatrix}\begin{bmatrix} x_T \\ x_N \\ x_S \end{bmatrix} + \begin{bmatrix} \xi_T \\ \xi_N \\ \xi_S \end{bmatrix}, \tag{2.5}$$

where x_T, x_N, and x_S represent the variables within the TP, NP, and SP, respectively. In the Full LIM, the dynamics of the TP are:

$$\frac{dx_T}{dt} = \boldsymbol{L_{TT}} x_T + \boldsymbol{L_{NT}} x_N + \boldsymbol{L_{ST}} x_S + \xi_T. \tag{2.6}$$

Equation 2.5 can be used to identify the sub-matrices of $\boldsymbol{L}$ that encapsulate internal TP processes ($\boldsymbol{L_{TT}}$), internal NP processes ($\boldsymbol{L_{NN}}$), internal SP processes ($\boldsymbol{L_{SS}}$), coupling dynamics between TP and NP ($\boldsymbol{L_{NT}}$ and $\boldsymbol{L_{TN}}$), coupling dynamics between TP and SP ($\boldsymbol{L_{ST}}$ and $\boldsymbol{L_{TS}}$) and coupling dynamics between NP and SP ($\boldsymbol{L_{NS}}$ and $\boldsymbol{L_{SN}}$). Based on the different dynamics that different sub-matrices represent, we remove all the effects of coupling between tropical Pacific and extratropical Pacific by constructing a new operator, where only the local dynamics $\boldsymbol{L_{TT}}$, $\boldsymbol{L_{NN}}$ and $\boldsymbol{L_{SS}}$ are retained in $\boldsymbol{L}$. The new LIM system is named Tropical-Pacific-only LIM (TP-only LIM), where the TP system is controlled only by the local dynamics:

$$\frac{dx_T}{dt} = \boldsymbol{L_{TT}} x_T + \xi_T. \tag{2.7}$$

Similarly, by setting $\boldsymbol{L_{ST}} = \boldsymbol{L_{TS}} = \boldsymbol{L_{NS}} = \boldsymbol{L_{SN}} = 0$ in $\boldsymbol{L}$, we remove the coupling effects between TP and SP, constructing the Tropical Pacific-North Pacific LIM (TP-NP LIM), where the TP is described as:

$$\frac{dx_T}{dt} = \boldsymbol{L_{TT}} x_T + \boldsymbol{L_{NT}} x_N + \xi_T. \tag{2.8}$$

Finally, to remove the coupling between TP and NP, we zero out $\boldsymbol{L_{NT}}$, $\boldsymbol{L_{TN}}$, $\boldsymbol{L_{NS}}$, and $\boldsymbol{L_{SN}}$ in $\boldsymbol{L}$, and build the Tropical Pacific-South Pacific LIM (TP-SP LIM), where the TP is described as:

$$\frac{dx_T}{dt} = \boldsymbol{L_{TT}} x_T + \boldsymbol{L_{ST}} x_S + \xi_T. \tag{2.9}$$

Different EOF truncations of SST and SSH anomalies in TP, NP, and SP to define the state vector of Full-LIM are examined to confirm the robustness of the Full-LIM and decoupled LIMs. We find that the main results are not qualitatively changed with different EOF truncations (see and Figure S4 in Supporting Information S1).

2.4. Seasonal Forecast Skill and Growth Calculations in LIM

LIM predictions (e.g., Alexander et al., 2008) are obtained as:

$$\mathrm{x(t+\tau) = exp(\mathbf{L}\tau)x(t) = \mathbf{G}(\tau)x(t),} \tag{2.10}$$

where $\mathbf{G}(\tau) = \exp(\mathbf{L}\tau)$ is the propagator. To explore the seasonal forecast skill, we forecast x from different initial months of each year. For example, from each year's January, we forecast forward using Equation 2.10 to obtain the predicted variables for the following months. For each LIM, the correlation coefficients (ACC) between the predicted ENSO indices and the observed ENSO indices from 1958 to 2015 at different lag times are calculated to examine the forecast skill of ENSO.

The LIM can also be used to identify the "optimal" initial condition for maximizing the amplification of the tropical SST anomalies (e.g., PS95; D. J. Vimont et al., 2014; Capotondi & Sardeshmukh, 2015; D. J. Vimont et al., 2022). The optimal initial condition obtained through singular value decomposition (SVD) of the system propagator $\boldsymbol{G}(\tau) = exp(\boldsymbol{L}\tau)$ to maximize the L_2 norm of tropical SST anomalies (i.e., $\boldsymbol{SST_T}^T \boldsymbol{SST_T}$), is also the most relevant initial condition for ENSO development. The SVD analysis generates the dominant pair of normalized singular vectors u_1, v_1 and the corresponding maximum singular value λ_1. At time $t = \tau$, the initial condition v_1 leads to the anomaly: $\mathbf{G}(\tau)v_1 = \lambda_1 u_1$. The variation of the maximum possible anomaly growth factor $\lambda_1^2(\tau)$ as a function of τ is defined as the "Maximum amplification" (MA) curve (PS95).

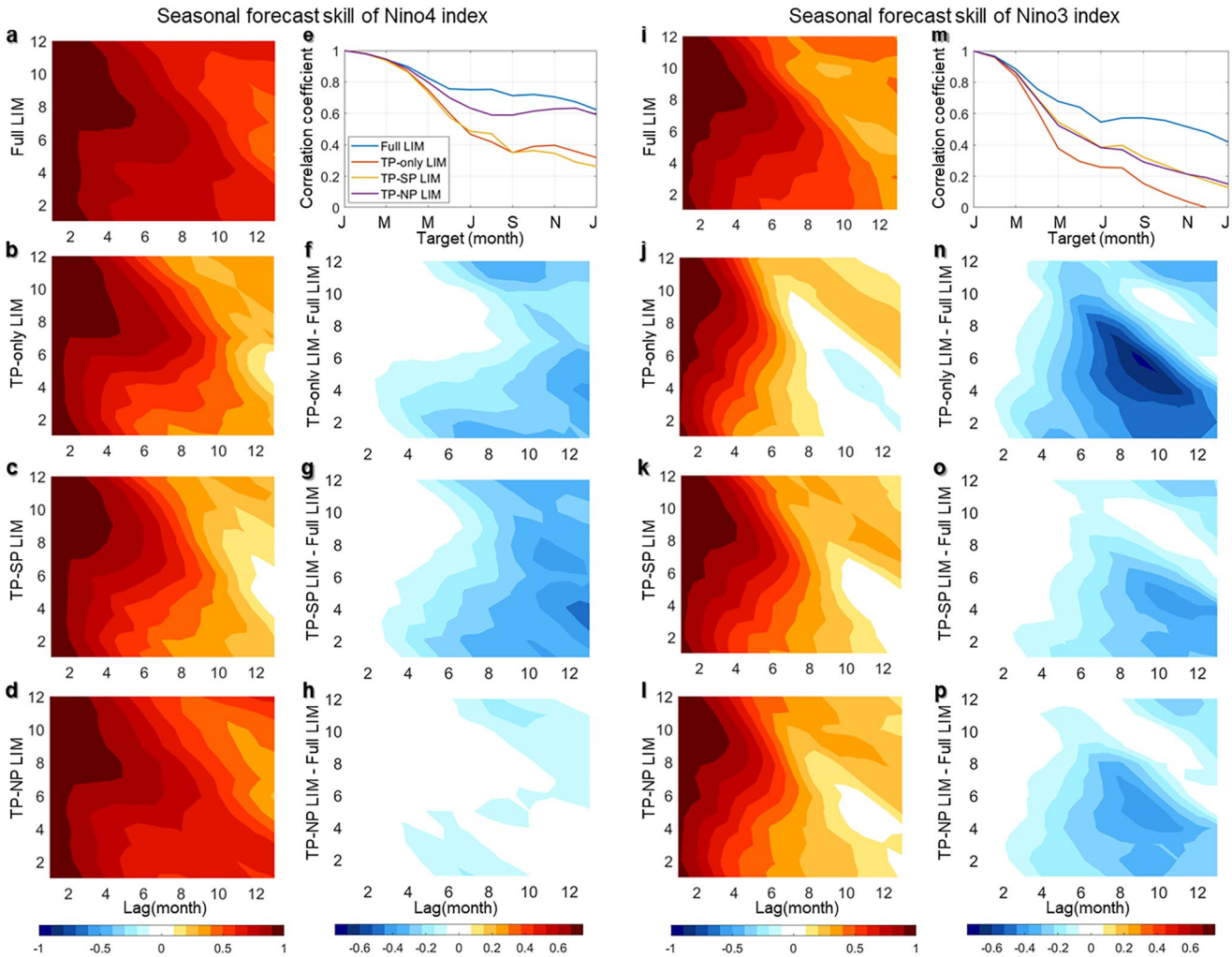

Figure 1. The seasonal correlation forecast skill of the Niño4 index as a function of the initial calendar month (*y*-axis) and lag month (*x*-axis) predicted by (a) Full LIM, (b) TP-only LIM, (c) TP-SP LIM and (d) TP-NP LIM. (e) Correlation forecast skills of the Niño4 index predicted from January in Full LIM (blue line), TP-only LIM (red line), TP-SP LIM (orange line), and TP-NP LIM (purple line). Difference of seasonal Niño4 index forecast skill between (f) TP-only LIM and Full LIM, (g) TP-SP LIM and Full LIM, (h) TP-NP LIM and Full LIM. (i–p) Same as (a)–(h), but for Niño3 index.

3. The Role of Extratropical Pacific in ENSO Diversity of SPB

3.1. Seasonal Forecast Skills Using Different LIMs

To explore the impacts of extratropical Pacific on the SPB, seasonal correlation forecast skills of the ENSO indices predicted by different LIMs are shown in Figure 1. The predictability maps represent the forecast skills as a function of the initial calendar month (*y*-axis) and lag month (*x*-axis) for Niño4 index (Figs. 1, a–d) and Niño3 index (Figure 1, i–l), respectively. In general, CP and EP ENSO (including or excluding the effect of extratropical Pacific) exhibit a distinct SPB feature (Figure 1), as a result of the seasonal variation of the background conditions in the tropical Pacific (Y. Jin et al., 2019). However, the role of extratropical Pacific in weakening SPB can be identified in Figure 1 (e.g., Figure 1a vs. Figure 1b).

For the CP-ENSO (Niño4 index), the full LIM, which includes the impacts of extratropical Pacific, exhibits the best forecast skill (Figure 1a) compared to other LIMs (Figures 1b–1d). For instance, the ACC is still about 0.7 at 6 months lead time when the initial month is January (Figure 1a). By decoupling the tropical and extratropical Pacific, the forecast skill is greatly reduced compared to the full LIM (Figure 1a vs. Figure 1b, see also Figure 1f), especially when the initial months are in boreal spring (Figure 1f), leading to a much stronger SPB in TP-only LIM (Figure 1b). In TP-only LIM, the ACC is about 0.4 at 6 months lead time when the initial month is January

(Figure 1b), which is significantly smaller than that in the Full LIM (0.7 in Figure 1a). To demonstrate which hemisphere is more important for CP-ENSO SPB, we further investigate Niño4 index forecast skill in TP-SP LIM/TP-NP LIM where the tropical Pacific is only coupled with South Pacific/North Pacific (Figures 1c and 1d). When the interaction between the tropical Pacific and South Pacific is considered, there is no much improvement in forecast skill compared to the TP-only LIM (Figure 1b vs. Figure 1c). However, when the impacts of the North Pacific are considered, the TP-NP LIM shows greatly enhanced forecast skill compared to TP-only LIM (Figure 1d vs. Figure 1b). The forecast skill of TP-NP LIM is comparable to that of the Full LIM (Figure 1d vs. Figure 1a, see also Figure 1h), which also suggests the important role of the North Pacific in the predictability of CP-ENSO.

To further identify the roles of the extratropical Pacific in SPB, we compare the Niño4 index forecast skill predicted from January in different LIMs (Figure 1e) and find that the dynamics between tropical Pacific and North Pacific can greatly weaken the SPB of CP-ENSO. The ACC skill in TP-only LIM (red line in Figure 1e) shows a stronger SPB, decreasing much faster than that in the Full LIM (blue line in Figure 1e) after April. When the dynamics of the South Pacific are added, the TP-SP LIM (orange line in Figure 1e) shows similar forecast skill to the TP-only LIM (red line in Figure 1e). However, when we include the dynamics of the North Pacific, the prediction of the Niño4 index is significantly improved during the SPB (purple line in Figure 1e), with ACC being slightly lower than that in the Full LIM (blue line in Figure 1e). Similar results can be obtained when the initial month is February or March (Figure S5a–b in Supporting Information S1) or using different CP indexes (Figure S6a–e in Supporting Information S1).

For EP-ENSO (Niño3 index), when tropical Pacific and extratropical Pacific are decoupled (TP-only LIM, Figure 1j), the seasonal forecast skill is significantly decreased compared to the coupled system (Full LIM, Figure 1i). The difference of forecast skill between Full LIM and TP-only LIM is most evident during the SPB season (initial month from January to May, Figure 1n) and is much smaller during boreal summer and autumn (initial month from July to November, Figure 1n). Notably, the SPB is much stronger in all decoupled LIMs (Figure 1j–l) compared to the Full LIM (Figure 1i), suggesting that both North Pacific and South Pacific are important for the EP-ENSO SPB. Similar results can be obtained from the comparison of the ACC at different lead times when the initial month is January (Figure 1m). The ACC skill in TP-only LIM (red line in Figure 1m) shows a much stronger SPB than the Full LIM (blue line in Figure 1m) after March. The predictabilities of the Niño3 index in TP-SP LIM and TP-NP LIM are similar to each other (yellow line and purple line in Figure 1m), suggesting a comparable and independent influence of the NP and SP on the forecast skill of EP-ENSO. Similarly, the initial month (e.g., February or March in Figure S5e-f in Supporting Information S1) or different EP indexes (Figure S6f–j in Supporting Information S1) do not qualitatively change the results. Recent studies indicated that the EP-ENSO has a relatively higher prediction skill than the CP-ENSO based on dynamical models (e.g., Jeong et al., 2012, 2015; H. L. Ren et al., 2017; Yang & Jiang, 2014; Zhu et al., 2015). However, although both NP and SP contribute to EP-ENSO predictability, our results show that the ACC forecast skill of EP-ENSO in Full LIM is overall lower than that of CP-ENSO (Figure 1e vs. Figure 1m), which is consistent with previous studies using statistical models (e.g., Tseng et al., 2022).

Note that the impact of the extratropical Pacific on ENSO predictability is not limited to the SPB season but is more effective during the SPB season (Figures 1f–1h and Figure 1n–p). The differences between the Full LIM and the decoupled LIMs are shown in Figures 1f–1h and Figure 1n–p. The impact of the extratropical Pacific on ENSO predictability is more effective during the SPB season (initial month from January to May, Figure 1f and Figure 1n), and is less effective during boreal summer and autumn (initial months from June to November). This point can be further identified in Figure S5 in Supporting Information S1. Forecast skills starting from June and October (Figures S5c–d and S5g–h in Supporting Information S1) exhibit the extratropical impacts on ENSO predictability during other seasons (boreal summer and autumn), but are not as profound as those during the SPB season (Figures S5a–b and S5e–f in Supporting Information S1). This is consistent with the fact that the NPMM dynamics mostly trigger ENSO in boreal spring (e.g., Chiang & Vimont, 2004). The seasonal cycle of the background state in the tropical Pacific can lead to the SPB (An & Wang, 2001; Y. Jin et al., 2019; A. F. Levine and McPhaden, 2015). For example, a deeper thermocline of the tropical Pacific in spring can induce the SPB. By including the influence of the extratropical Pacific, stronger wind anomalies (e.g., caused by NPMM) can be generated in the tropical Pacific during spring, leading to stronger thermocline and zonal advective feedbacks and a larger signal in crossing the SPB.

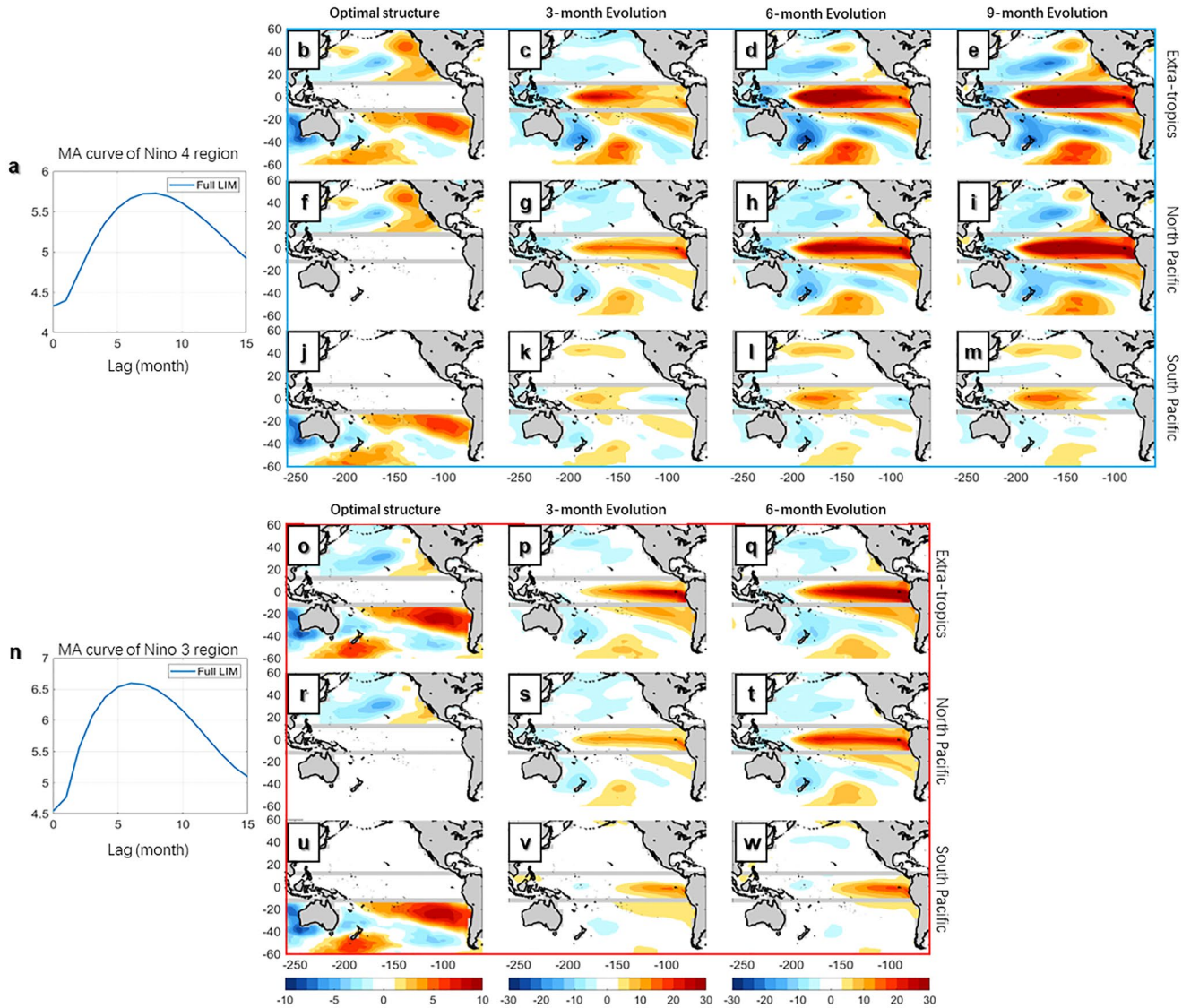

Figure 2. (a) The "MA Curve" of SST variances in Niño4 region in Full LIM. (b) The 8-month extratropical optimal initial structure of SST variances in Niño4 region and (c)–(e) the time evolution from 3 to 9 months. (f)–(i) and (j–m) are same with (b)–(e), expect for the evolution of North and South Pacific optimal initial structures, respectively. (n) Similar to (a) but for Niño3 region. (o–q) 6-month extratropical optimal initial structure of Niño3 region and its time evolution from 3 to 6 months. (r–t) and (u–w) are same as (o–q) expect for the evolution of North and South Pacific optimal initial structures, respectively.

In summary, the extratropical Pacific can significantly weaken ENSO SPB. Specifically, for CP-ENSO, the North Pacific is much more important than the South Pacific in crossing the SPB, while the North and South Pacific tend to play an equally essential role in weakening EP-ENSO SPB.

3.2. The Optimum Initial Condition of Central and Eastern Tropical Pacific

To clarify why the northern and southern extratropical Pacific play different roles in predicting CP-ENSO like mode and EP-ENSO like mode, we compare the extratropical optimum initial conditions for the growth of SST anomalies in the Niño3 and Niño4 regions in the Full LIM, and explore how they evolve with time. Note that since the Niño3 and Niño4 indices are not independent, the mature patterns develop as a combination of EP and CP patterns (Figures 2e and 2q) rather than typical EP and CP spatial structures. The specific mathematical procedure is introduced in Text S4 in Supporting Information S1.

First, we show how the extratropical initial conditions can evolve into a CP- ENSO like mode (Figures 2b–2e). The MA curve for SST anomaly growth in the Niño4 region (Figure 2a) shows that the maximum growth is achieved at a lag of about 8 months, which is consistent with typical lags between extratropical precursor dynamics and ENSO (9–10 months) (Ding et al., 2015b, 2017; Zhao & Di Lorenzo, 2020). Therefore, we chose $\tau = 8$ months for the Niño4 region to calculate the optimal initial conditions in the extratropical Pacific and see how these conditions evolve. Note that the extratropical optimal initial conditions (Figure 2b) resemble the typical foot-printing pattern in the North Pacific (D. J. Vimont et al., 2001, 2003a; 2003b) and the quadrupole structure in the South Pacific (Ding, Li, & Tseng, 2015), suggesting that these modes are important for ENSO development. We further integrate Equation 2.1 using the extratropical initial condition (with no signal in the tropical Pacific) to see their time evolution. After 3 months, a distinct warming signal can be seen in the central tropical Pacific (Figure 2c), which is amplified in the tropical Pacific (Figure 2d) and finally evolves into a mature ENSO mode after 9 months (Figure 2e). This suggests that even without an initial signal in the tropical Pacific, perturbations in the extratropical Pacific (e.g., the westerly wind anomalies) could induce strong SST anomalies in the Niño4 region.

To determine the individual impact of the North Pacific or South Pacific, we compare the ENSO progression developing from the northern (Figures 2f–2i) or the southern extratropical initial condition (Figure 2j–m). Note that the addition of the evolution from each hemisphere equals to the evolution from both hemispheres (e.g., Figu re 2i + Figure 2m = Figure 2e). The North Pacific initial condition (Figure 2f) can drive a strong warming signal in the central tropical Pacific (Figure 2i) with comparable amplitude to Figure 2e after 9 months of evolution. It indicates the important role that the North Pacific plays in the development of SSTa in the Niño4 region, which is consistent with Stuecker (2018). On the other hand, after 9 months of evolution, the warming anomalies in the central tropical Pacific developed from the South Pacific initial condition (Figure 2m) are much weaker compared to Figure 2e, which indicates that the South Pacific is less important for the development of SSTa in Niño4 region. Therefore, dynamics in North Pacific contribute more to the development and prediction of CP-ENSO-like mode compared to the South Pacific, explaining the dramatic drop of the Niño4 index forecast skill in boreal spring when we neglect the North Pacific dynamics (e.g., the orange line in Figure 1e).

Both North Pacific and South Pacific are important for the development of EP-ENSO-like mode (Figure 2o–w). The extratropical initial condition for SST anomaly growth in the Niño3 region (Figure 2o) is similar to that for the Niño4 region (Figure 2b). The extratropical dynamics drive EP-ENSO-like variance in the tropical Pacific after 3 months (Figure 2p), which is further developed into an EP-ENSO-like mode after 6 months (Figure 2q). Note that here we show the evolution for a 6 months growth period as the maximum growth rate of the MA curve in the Niño3 region (Figure 2n) occurs at about 6 months. The northern and southern extratropical initial structures (Figure 2r vs. Figure 2u) can drive EP-ENSO-like mode individually with comparable amplitude in the final condition (6-month evolution, Figure 2t vs. Figure 2w) in the eastern Pacific, which means North Pacific and South Pacific are almost equally important to the development of EP-ENSO like mode.

Note here that the North Pacific initial condition drives warming both in the central and eastern Pacific (Figures 2i and 2t), while the South Pacific initial condition may play an important role in determining CP-ENSO or EP-ENSO like pattern (Figures 2m and 2w). For the Niño4 region, in the mature pattern developing from the NP initial condition only (Figure 2i), the warm anomalies are stronger in eastern Pacific and weaker in central Pacific compared to the mature pattern of the extratropical initial condition (Figure 2e, which indicates the warm anomalies in the western and central Pacific). However, driven by the South Pacific initial condition (Figure 2m), the positive anomalies in the central Pacific and weak negative anomalies in the eastern Pacific occur, which is similar with the pattern of Figure 2e. Similarly, for the Niño3 region, the North Pacific initial condition drives warm anomalies evenly along the equator (Figure 2t), while the South Pacific drives the typical EP-ENSO pattern with warm signal only exists in eastern Pacific region (Figure 2w). As such, the South Pacific may play a role in ENSO diversity.

4. The Asymmetrical Role of Extratropical Pacific in the SPB of ENSO

We next explore how extratropical Pacific dynamics impact the prediction of different phases of ENSO (i.e., El Niño and La Niña). The Niño 3.4 index forecast skill for El Niño developing years (black lines) and La Niña developing years (blue lines) using Full LIM (solid lines) and TP-only LIM (dashed lines) are shown in Figure 3.

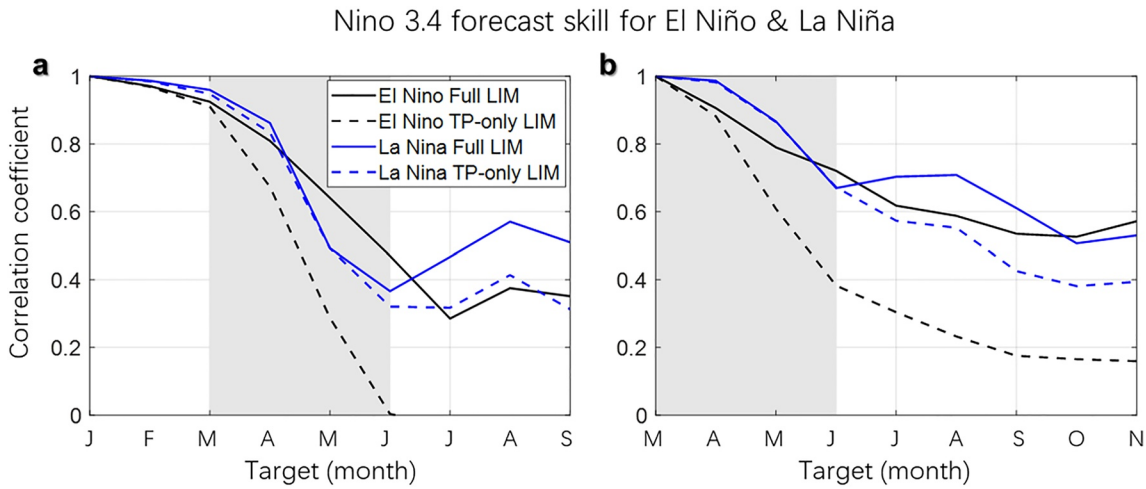

Figure 3. Niño3.4 forecast skill of El Niño years predicted by Full LIM (black solid line), TP-only LIM (black dashed line) and that of La Niña years predicted by Full LIM (blue solid line), TP-only LIM (blue dashed line) when initial month is (a) January and (b) March. Gray shading indicates the targeted (predicted) months from March to June, which is corresponding to the SPB.

For La Niña, TP-only LIM (blue dashed line in Figure 3a) and Full LIM (blue solid line in Figure 3a) show similar Niño3.4 index forecast skills during boreal spring (i.e., similar SPB), suggesting that the extratropical Pacific plays a less important role in predicting La Niña events. However, including the interactions between tropical Pacific and extratropical Pacific can greatly improve the predictability of El Niño during the SPB (black solid line vs. black dashed line in Figure 3a). Therefore, the role of the extratropical Pacific for predicting ENSO events is asymmetric. Particularly, the extratropical Pacific significantly influences the predictability of El Niño events during boreal spring, while the extratropical impact on La Niña SPB is much weaker. Similar results can be obtained when the initial month is March (Figure 3b). This is consistent with the finding of Amaya et al. (2019) that the relationship between NPMM and ENSO is more consistent for El Niño events than La Niña events. We further study the individual contribution of North Pacific and South Pacific and find that they are almost equally important for the prediction of El Niño (Figure S7a-b in Supporting Information S1). On the other hand, this individual effect is limited for predicting La Niña (Figure S7c–d in Supporting Information S1). Previous studies have shown that the equatorial heat content plays a more important role in predicting La Niña compared to El Niño (Planton et al., 2021), suggesting that subsurface information from the tropical Pacific may be sufficient for crossing the La Niña SPB.

Since the LIM dynamical operator L only contains linear processes, the asymmetry of extratropical impacts on different ENSO phases is caused by the asymmetry in the initial conditions. To determine how the extratropical dynamics influence El Niño and La Niña events, composite maps of seasonal SST anomalies and the corresponding wind stress anomalies in the El Niño years and La Niña years are shown (Figure 4). In the boreal spring of El Niño years (January-March, JFM; Figure 4a), warm SST and westerly wind anomalies can be seen in the northern subtropical Pacific region (red square in Figure 4a). These anomalies may propagate southwestward toward the equator through the wind-evaporation-SST (WES) feedback (Xie & Philander, 1994) and result in strong equatorial westerly wind anomalies, that can energize El Nino events (D. J. Vimont et al., 2001, 2003a,b) in the following seasons (Figures 4b–4d). The extra-tropical wind anomalies can also create heat content anomalies in the central equatorial Pacific, conducive to El Nino development, by altering the meridional thermocline transport, a process known as "trade wind charging" (Anderson, Perez, & Karspeck, 2013). However, in the JFM of La Niña (Figure 4e), SST cooling signal and easterly wind anomalies are stronger in the western tropical region (red square in Figure 4e) rather than in the northern extratropical Pacific, indicating that the extratropical information plays a less important role in the forecast of La Niña compared to El Niño. Thus, the development of an El Niño appears to be strongly controlled by the extra-tropical precursors, which contribute to weakening the SPB, while La Niña events seem to be more influenced by equatorial subsurface conditions.

Another possible explanation is the asymmetrical mechanism of El Niño/La Niña in the tropical Pacific (Clarke & Zhang, 2019). Specifically, during El Niño, westerly equatorial wind anomalies push the warm pool eastward.

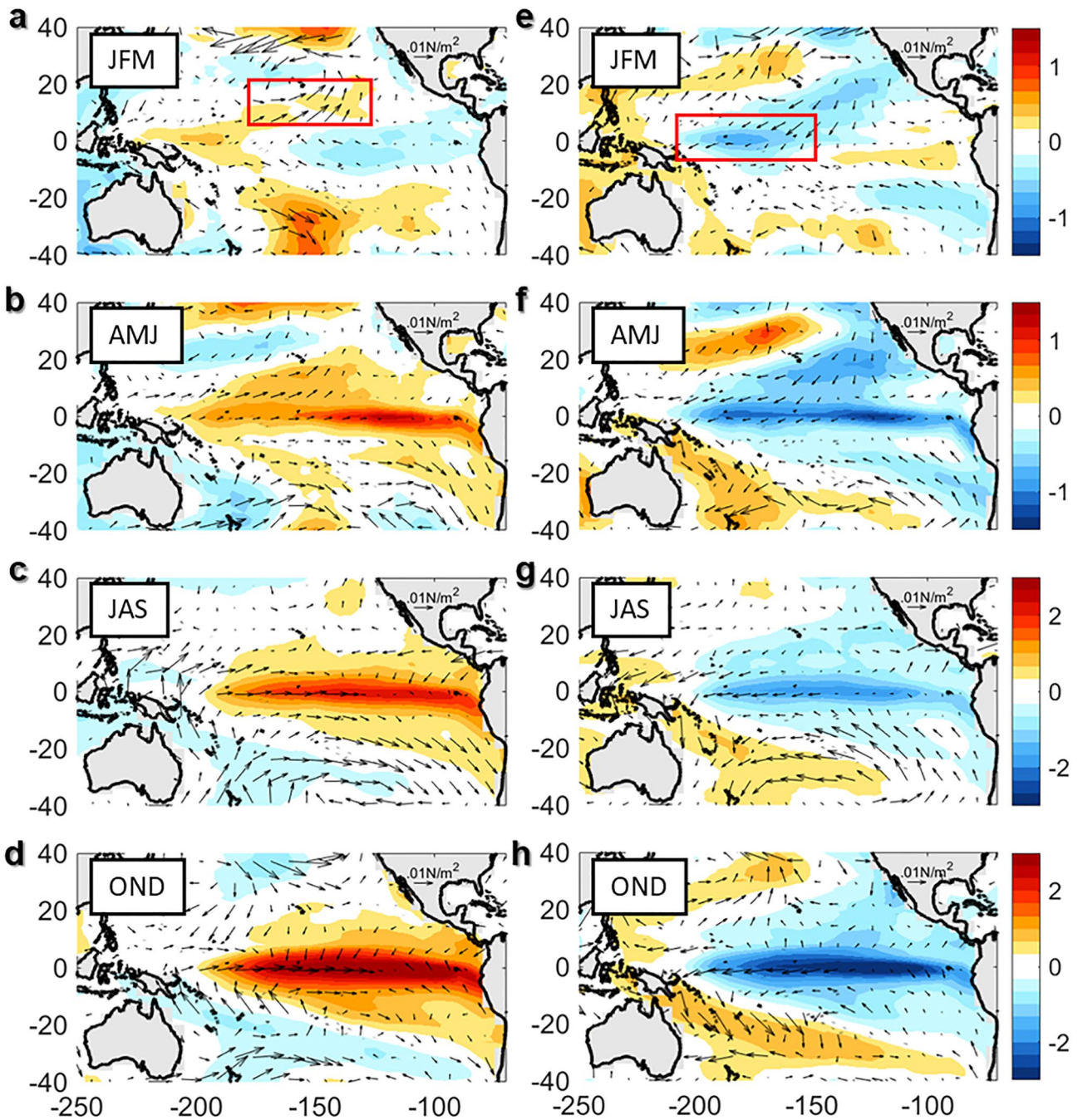

Figure 4. The composites of seasonal SST anomalies (shadings) and wind stress anomalies (arrows) of El Niño years in (a) January–March (JFM), (b) April–June (AMS), (c) July–September (JAS) and (d) October–December (OND). (e)–(h) Similar to (a)–(d) but for La Niña years.

In the mature phase, the westerly wind anomalies shift south of the equator (Harrison, 1987) following the warmest water south of the equator (Harrison & Vecchi, 1999) in the Southern Hemisphere summer in December–February. With the removal of wind forcing, the sea level and thermocline anomalies in the eastern equatorial Pacific decrease, resulting in an anomalous westward equatorial flow which tends to push the warm pool westward (X. Zhang and Clarke, 2017) and usually drives a La Niña during March–June. However, during La Niña, the anomalously negative sea level in the eastern equatorial Pacific typically does not change as much, and the negative feedback is not as strong. Therefore, La Niña or weakly negative conditions instead of El Niños tend to follow a La Niña the next year. In this case, the extratropical forcing is important to kick the La Niña system to

El Niños and that may be a reason why the extratropical Pacific is more important to the prediction of El Niños compared to La Niñas.

5. Summary and Discussion

Using a linear dynamical model (LIM), we explore the distinct impacts of extratropical Pacific on ENSO SPB strength. We find that North Pacific dynamics are very important to weaken the SPB of CP-ENSO while the joint effects of northern and southern extratropical Pacific are important for crossing EP-ENSO SPB. By comparing the ENSO evolution developing from NP/SP initial condition (Figure 2), our results emphasize that the South Pacific initial condition may play an important role in determining ENSO diversity. Meanwhile, the extratropical Pacific can significantly improve the prediction of El Niño events during boreal spring, while the tropical Pacific subsurface conditions seem to be more essential for the prediction of La Niña. Our results suggest that El Niño can be more predictable and the SPB can be weakened when the extratropical Pacific dynamics are appropriately considered.

Note that here we emphasize the role of the extratropical Pacific in crossing the SPB of ENSO. Previous studies have shown the impacts of extratropical Pacific on the predictability of ENSO (e.g., Chen et al., 2020; Pegion et al., 2020; Tseng et al., 2022). A more recent paper also discussed the influence of the north Pacific Victoria mode on the spring persistence barrier of ENSO (Shi et al., 2022). However, the relative effects of both the north and south Pacific on ENSO SPB are less mentioned. These extratropical dynamics identified by the LIM can drive ENSO-like variances in the tropical Pacific (Figure 2), and contribute to the forecast skill of ENSO during the SPB. Therefore, CP-ENSO and EP-ENSO tend to experience much stronger SPB without the impacts of the extratropical Pacific.

Our results also suggest the different roles of the extratropical Pacific in predicting El Niño and La Niña. The La Niña events are less impacted by the extratropical Pacific compared to the El Niño events. Thus, if only tropical dynamics are considered (e.g., Planton et al., 2021), the predictability of La Niña may be higher than that of El Niño (blue dashed line and black dashed line in Figure 3). These results highlight the importance of including extratropical dynamics to predict El Niño events.

We further explore the asymmetry of the extratropical impact on the prediction of CP-ENSO events and EP-ENSO events (Figure S8 in Supporting Information S1). By adding the information of the extratropical Pacific, the prediction skill of CP El Niño drops much slower during the spring. However, this information is less important for both CP La Niña and EP events (including El Niño events and La Niña events). Overall, the asymmetrical role of extratropical Pacific is more distinct for CP events than EP events. Note that the number of CP events is small according to our definition (see Text S3 in Supporting Information S1) so the result may lack robustness. However, this result is consistent with previous studies that extratropical ENSO precursors have a stronger connection to CP-ENSO compared to EP-ENSO (Capotondi & Ricciardulli, 2021; Pegion et al., 2020). Previous studies also have demonstrated a stronger impact from the northern extratropics (e.g., the NPMM, consisting of SST anomalies extending from Baja California to the central-western equatorial Pacific) for CP-ENSO than EP-ENSO (Amaya et al., 2019; D. J. Vimont et al., 2014; Yu & Kim, 2011).

LIM is a linear dynamical model, in which only fast nonlinearities are captured by the stochastic term ξ in Equation 2.1. However, nonlinear processes may also play an important role in ENSO prediction (e.g., A. Levine et al., 2016). As such, the role of the extratropical Pacific in ENSO SPB should be further examined using nonlinear models (e.g., coupled general circulation models). Another interesting aspect of this problem is the possible decadal modulation of the extratropical Pacific influence on the tropical Pacific. Since data records sufficiently long to capture decadal variations are needed to address this problem, century-long climate model simulations may be suitable candidates for examining decadal variations of the extratropical impacts on ENSO predictability in future studies.

Data Availability Statement

The ORAS4 output can be downloaded from: https://www.cen.uni-hamburg.de/en/icdc/data/ocean/easy-init-ocean/ecmwf-ocean-reanalysis-system-4-oras4.html. The NCEP 10-m wind components are obtained from: https://psl.noaa.gov/data/gridded/data.ncep.reanalysis.derived.surfaceflux.html.

Acknowledgments
We thank two anonymous reviewers and editor for their constructive comments on this paper. This work is supported by Shandong Provincial Natural Science Foundation, China, ZR202102240275 and Chinese NSFC41906009.

References

Alexander, M. A., Bladé, I., Newman, M., Lanzante, J. R., Lau, N.-C., & Scott, J. D. (2002). The atmospheric bridge: The influence of ENSO teleconnections on air–sea interaction over the global oceans. *Journal of Climate*, *15*, 2205–2231. https://doi.org/10.1175/1520-0442(2002)015<2205:tabtio>2.0.co;2

Alexander, M. A., Matrosova, L., Penland, C., Scott, J. D., & Chang, P. (2008). Forecasting Pacific SSTs: Linear inverse model predictions of the PDO. *Journal of Climate*, *21*, 385–402. https://doi.org/10.1175/2007jcli1849.1

Amaya, D. J., Kosaka, Y., Zhou, W., Zhang, Y., Xie, S., & Miller, A. J. (2019). The North Pacific pacemaker effect on historical ENSO and its mechanisms. *Journal of Climate*, *32*(22), 7643–7661. https://doi.org/10.1175/jcli-d-19-0040.1

An, S., & Wang, B. (2001). Mechanisms of locking of the El Niño and La Niña mature phases to boreal winter. *Journal of Climate*, *14*(9), 2164–2176. https://doi.org/10.1175/1520-0442(2001)014<2164:molote>2.0.co;2

Anderson, B. T., Furtado, J. C., Cobb, K. M., & Di Lorenzo, E. (2013a). Extratropical forcing of El Niño–southern oscillation asymmetry. *Geophysical Research Letters*, *40*(18), 4916–4921. https://doi.org/10.1002/grl.50951

Anderson, B. T., Perez, R. C., & Karspeck, A. (2013). Triggering of El Niño onset through trade wind–induced charging of the equatorial Pacific. *Geophysical Research Letters*, *40*, 1212–1216. https://doi.org/10.1002/grl.50200

Balmaseda, M. A., Mogensen, K., & Weaver, A. T. (2013). Evaluation of the ECMWF ocean reanalysis system ORAS4. *Quarterly Journal of the Royal Meteorological Society*, *139*, 1132–1161. https://doi.org/10.1002/qj.2063

Capotondi, A., Deser, C., Phillips, A. S., Okumura, Y., & Larson, S. M. (2020). ENSO and Pacific decadal variability in the community Earth system model version 2. *Journal of Advances in Modeling Earth Systems*, *12*, e2019MS002022. https://doi.org/10.1029/2019ms002022

Capotondi, A., & Ricciardulli, L. (2021). The influence of pacific winds on ENSO diversity. *Scientific Reports*, *11*, 18672. https://doi.org/10.1038/s41598-021-97963-4

Capotondi, A., & Sardeshmukh, P. D. (2015). Optimal precursors of different types of ENSO events. *Geophysical Research Letters*, *42*, 9952–9960. https://doi.org/10.1002/2015GL066171

Capotondi, A., Wittenberg, A. T., Kug, J.-S., Takahashi, K., & McPhaden, M. (2021). ENSO diversity. In M. J. McPhaden, A. Santoso, & W. Cai (Eds.), *El Niño southern oscillation in a changing climate* (pp. 65–86). American Geophysical Union (AGU).

Capotondi, A., Wittenberg, A. T., Newman, M., Di Lorenzo, E., Yu, J.-Y., Braconnot, P., et al. (2015). Understanding ENSO diversity. *Bulletin of the American Meteorological Society*, *96*(6), 921–938. https://doi.org/10.1175/bams-d-13-00117.1

Chang, P., Zhang, L., Saravanan, R., Vimont, D. J., Chiang, J. C. H., Ji, L., et al. (2007). Pacific meridional mode and El Niño—Southern oscillation. *Geophysical Research Letters*, *34*, L16608. https://doi.org/10.1029/2007GL030302

Chen, H. C., Tseng, Y. H., Hu, Z. Z., & Ding, R. (2020). Enhancing the ENSO predictability beyond the spring barrier. *Scientific Reports*, *10*, 984. https://doi.org/10.1038/s41598-020-57853-7

Chiang, J. C. H., & Vimont, D. J. (2004). Analogous Pacific and Atlantic meridional modes of tropical atmosphere–ocean variability. *Journal of Climate*, *17*(21), 4143–4158. https://doi.org/10.1175/jcli4953.1

Clarke, A. J., & Zhang, X. (2019). On the physics of the warm water volume and El Niño/La Niña predictability. *Journal of Physical Oceanography*, *49*(6), 1541–1560. https://doi.org/10.1175/jpo-d-18-0144.1

Deser, C., Phillips, A. S., Tomas, R. A., Okumura, Y. M., Alexander, M. A., Capotondi, A., et al. (2012). ENSO and Pacific decadal variability in the community climate system model version 4. *Journal of Climate*, *25*(8), 2622–2651. https://doi.org/10.1175/jcli-d-11-00301.1

Di Lorenzo, E., Cobb, K. M., Furtado, J. C., Schneider, N., Anderson, B. T., Bracco, A., et al. (2010). Central pacific El Nino and decadal climate change in the North Pacific ocean. *Nature Geoscience*, *3*(11), 762–765. https://doi.org/10.1038/ngeo984

Ding, R., Li, J., & Tseng, Y. h. (2015). The impact of South Pacific extratropical forcing on ENSO and comparisons with the North Pacific. *Climate Dynamics*, *44*, 2017–2034. https://doi.org/10.1007/s00382-014-2303-5

Ding, R., Li, J., Tseng, Y.-h., Sun, C., & Guo, Y. (2015). The Victoria mode in the North Pacific linking extratropical sea level pressure variations to ENSO. *Journal of Geophysical Research: Atmospheres*, *120*, 27–45. https://doi.org/10.1002/2014JD022221

Ding, R., Li, J., Tseng, Y.-H., Sun, C., & Xie, F. (2017). Joint impact of North and South Pacific extratropical atmospheric variability on the onset of ENSO events. *Journal of Geophysical Research: Atmospheres*, *122*, 279–298. https://doi.org/10.1002/2016jd025502

Frankignoul, C., Gastineau, G., & Kwon, Y. O. (2017). Estimation of the SST response to anthropogenic and external forcing and its impact on the Atlantic multidecadal oscillation and the Pacific decadal oscillation. *Journal of Climate*, *30*(24), 9871–9895. https://doi.org/10.1175/jcli-d-17-0009.1

Harrison, D. E. (1987). Monthly mean island surface winds in the central tropical Pacific and El Niño events. *Monthly Weather Review*, *115*, 3133–3145. https://doi.org/10.1175/1520-0493(1987)115<3133:mmiswi>2.0.co;2

Harrison, D. E., & Vecchi, G. A. (1999). On the termination of El Niño. *Geophysical Research Letter*, *26*, 1593–1596. https://doi.org/10.1029/1999GL900316

Hou, M., Duan, W., & Zhi, X. (2019). Season-dependent predictability barrier for two types of El Niño revealed by an approach to data analysis for predictability. *Climate Dynamics*, *53*(9), 5561–5581. https://doi.org/10.1007/s00382-019-04888-w

Hou, Z., Li, J., Ding, R., Karamperidou, C., Duan, W., Liu, T., & Feng, J. (2018). Asymmetry of the predictability limit of the warm ENSO phase. *Geophysical Research Letters*, *45*(15), 7646–7653. https://doi.org/10.1029/2018gl077880

Jeong, H.-I., Ahn, J.-B., Lee, J.-Y., Alessandri, A., & Hendon, H. H. (2015). Interdecadal change of interannual variability and predictability of two types of ENSO. *Climate Dynamics*, *44*, 1073–1091. https://doi.org/10.1007/s00382-014-2127-3

Jeong, H.-I., Lee, D. Y., Ashok, K., Ahn, J.-B., Lee, J.-Y., Luo, J.-J., et al. (2012). Assessment of the APCC couple MME suite in predicting the distinctive climate impacts of two flavors of ENSO during boreal winter. *Climate Dynamics*, *39*, 475–493. https://doi.org/10.1007/s00382-012-1359-3

Jin, E. K., Kinter, J. L., Wang, B., Park, C.-K., Kang, I.-S., Kirtman, B. P., et al. (2008). Current status of ENSO prediction skill in coupled ocean–atmosphere models. *Climate Dynamics*, *31*(6), 647–664. https://doi.org/10.1007/s00382-008-0397-3

Jin, Y., & Liu, Z. (2021a). A theory of the spring persistence barrier on ENSO. Part I: The role of ENSO period. *Journal of Climate*, *34*(6), 2145–2155. https://doi.org/10.1175/jcli-d-20-0540.1

Jin, Y., & Liu, Z. (2021b). A theory of the spring persistence barrier on ENSO. Part II: Persistence barriers in SST and ocean heat content. *Journal of Climate*, *34*(13), 5555–5564. https://doi.org/10.1175/jcli-d-21-0070.1

Jin, Y., Liu, Z., He, C., & Zhao, Y. (2021). On the formation mechanism of the seasonal persistence barrier. *Journal of Climate*, *34*(2), 479–494. https://doi.org/10.1175/jcli-d-19-0502.1

Jin, Y., Liu, Z., Lu, Z., & He, C. (2019). Seasonal cycle of background in the tropical Pacific as a cause of ENSO spring persistence barrier. *Geophysical Research Letters*, *46*(22), 13371–13378. https://doi.org/10.1029/2019gl085205

Jin, Y., Lu, Z., & Liu, Z. (2020). Controls of spring persistence barrier strength in different ENSO regimes and implications for 21st century changes. *Geophysical Research Letters*, *47*(11), e2020GL088010. https://doi.org/10.1029/2020gl088010
Kalnay, E., Kanamitsu, M., Kistler, R., Collins, W., Deaven, D., Gandin, L., et al. (1996). The NCEP/NCAR 40-Year reanalysis project. *Bulletin of the American Meteorological Society*, *77*(3), 437–471. https://doi.org/10.1175/1520-0477(1996)077<0437:tnyrp>2.0.co;2
Levine, A., Jin, F. F., & McPhaden, M. J. (2016). Extreme noise–extreme El Niño: How state-dependent noise forcing creates El Niño–La Niña asymmetry. *Journal of Climate*, *29*(15), 5483–5499. https://doi.org/10.1175/jcli-d-16-0091.1
Levine, A. F., & McPhaden, M. J. (2015). The annual cycle in ENSO growth rate as a cause of the spring predictability barrier. *Geophysical Research Letters*, *42*(12), 5034–5041. https://doi.org/10.1002/2015gl064309
Liu, Z., & Di Lorenzo, E. (2018). Mechanisms and predictability of Pacific decadal variability. *Current Climate Change Reports*, *4*(2), 128–144. https://doi.org/10.1007/s40641-018-0090-5
Liu, Z., Jin, Y., & Rong, X. (2019). A theory for the seasonal predictability Barrier: Threshold, timing, and intensity. *Journal of Climate*, *32*(2), 423–443. https://doi.org/10.1175/jcli-d-18-0383.1
Mu, M., Duan, W., & Wang, B. (2007). Season-dependent dynamics of nonlinear optimal error growth and El Niño-Southern Oscillation predictability in a theoretical model. *Journal of Geophysical Research*, *112*, D10113. https://doi.org/10.1029/2005JD006981
Mu, M., Xu, H., & Duan, W. (2007b). A kind of initial errors related to "spring predictability barrier" for El Niño events in Zebiak-Cane model. *Geophysical Research Letters*, *34*, L03709. https://doi.org/10.1029/2006gl027412
Newman, M. (2007). Interannual to decadal predictability of tropical and North Pacific sea surface temperatures. *Journal of Climate*, *20*(11), 2333–2356. https://doi.org/10.1175/jcli4165.1
Newman, M., Alexander, M. A., & Scott, J. D. (2011). An empirical model of tropical ocean dynamics. *Climate Dynamics*, *37*(9), 1823–1841. https://doi.org/10.1007/s00382-011-1034-0
Pegion, K., Selman, C. M., Larson, S., Furtado, J. C., & Becker, E. J. (2020). The impact of the extratropics on ENSO diversity and predictability. *Climate Dynamics*, *54*, 4469–4484. https://doi.org/10.1007/s00382-020-05232-3
Penland, C., & Matrosova, L. (1994). A balance condition for stochastic numerical models with application to the El Nino-Southern Oscillation. *Journal of Climate*, *7*(9), 1352–1372. https://doi.org/10.1175/1520-0442(1994)007<1352:abcfsn>2.0.co;2
Penland, C., & Sardeshmukh, P. D. (1995). The optimal-growth of tropical sea-surface temperature anomalies. *Journal of Climate*, *8*(8), 1999–2024. https://doi.org/10.1175/1520-0442(1995)008<1999:togots>2.0.co;2
Planton, Y. Y., Vialard, J., Guilyardi, E., Lengaigne, M., & Mcphaden, M. J. (2021). The asymmetric influence of ocean heat content on ENSO predictability in the CNRM-CM5 coupled general circulation model. *Journal of Climate*, *34*(14), 5775–5793. https://doi.org/10.1175/jcli-d-20-0633.1
Ren, H. L., & Jin, F. F. (2011). Niño indices for two types of ENSO. *Geophysical Research Letters*, *38*(4), a–n. https://doi.org/10.1029/2010GL046031
Ren, H.-L., Jin, F.-F., Song, L., Lu, B., Tian, B., Zuo, J., et al. (2017). Prediction of primary climate variability modes in Beijing Climate Center. *Journal of Meteorological Research*, *31*, 204–223. https://doi.org/10.1007/s13351-017-6097-3
Shi, L., Ding, R., Hu, S., Li, L., Tseng, Y., & Li, X. (2022). Influence of the north pacific Victoria mode on the spring persistence barrier of ENSO. *Journal of Geophysical Research: Atmospheres*, *127*. https://doi.org/10.1029/2021JD036206
Stuecker, M. F. (2018). Revisiting the Pacific meridional mode. *Scientific Reports*, *8*(1), 1–9. https://doi.org/10.1038/s41598-018-21537-0
Tseng, Y.-H., Huang, J.-H., & Chen, H.-C. (2022). Improving the predictability of two types of ENSO by the characteristics of extratropical precursors. *Geophysical Research Letters*, *49*, e2021GL097190. https://doi.org/10.1029/2021GL097190
Vimont, D., Battisti, D., & Hirst, A. (2003a). The seasonal footprinting mechanism in the CSIRO general circulation models. *Journal of Climate*, *16*, 2653–2667. https://doi.org/10.1175/1520-0442(2003)016<2653:tsfmit>2.0.co;2
Vimont, D., Wallace, J., & Battisti, D. (2003b). The seasonal footprinting mechanism in the Pacific: Implications for ENSO. *Journal of Climate*, *16*, 2668–2675. https://doi.org/10.1175/1520-0442(2003)016<2668:tsfmit>2.0.co;2
Vimont, D. J., Alexander, M. A., & Newman, M. (2014). Optimal growth of central and east pacific ENSO events. *Geophysical Research Letters*, *41*(11). https://doi.org/10.1002/2014GL059997.1
Vimont, D. J., Battisti, D. S., & Hirst, A. C. (2001). Footprinting: A seasonal connection between the tropics and mid-latitudes. *Geophysical Research Letters*, *28*, 3923–3926. https://doi.org/10.1029/2001GL013435
Vimont, D. J., Newman, M., Battisti, D. S., & Shin, S. (2022). The role of seasonality and the ENSO mode in Central and East Pacific ENSO growth and evolution. *Journal of Climate*. (Published online ahead of print 2022). https://doi.org/10.1175/jcli-d-21-0599.1
Webster, P. J., & Yang, S. (1992). Monsoon and ENSO: Selectively interactive systems. *Quarterly Journal of the Royal Meteorological Society*, *118*(507), 877–926. https://doi.org/10.1002/QJ.49711850705
Wu, R., Kirtman, B. P., & Van den Dool, H. (2009). An analysis of ENSO prediction skill in the CFS retrospective forecasts. *Journal of Climate*, *22*(7), 1801–1818. https://doi.org/10.1175/2008jcli2565.1
Xie, S. P., & Philander, S. G. H. (1994). A coupled ocean-atmosphere model of relevance to the ITCZ in the eastern Pacific. *Tellus*, *46*, 340–350. https://doi.org/10.1034/j.1600-0870.1994.t01-1-00001.x
Xue, Y., Cane, M., Zebiak, S., & Blumenthal, M. (1994). On the prediction of ENSO: A study with a low-order Markov model. *Tellus*, *46*(4), 512–528. https://doi.org/10.1034/j.1600-0870.1994.00013.x
Yang, S., & Jiang, X. (2014). Prediction of eastern and central Pacific ENSO events and their impacts on east Asian climate by the NCEP climate forecast system. *Journal of Climate*, *27*, 4451–4472. https://doi.org/10.1175/jcli-d-13-00471.1
You, Y., & Furtado, J. C. (2018). The South Pacific meridional mode and its role in tropical pacific climate variability. *Journal of Climate*, *31*(24), 10141–10163. https://doi.org/10.1175/jcli-d-17-0860.1
Yu, J., & Kim, S. T. (2011). Relationships between extratropical sea level pressure variations and the Central Pacific and Eastern Pacific types of ENSO. *Journal of Climate*, *24*(3), 708–720. https://doi.org/10.1175/2010jcli3688.1
Zhang, H., Clement, A., & Di Nezio, P. (2014). The South pacific meridional mode: A mechanism for ENSO-like variability. *Journal of Climate*, *27*(2), 769–783. https://doi.org/10.1175/jcli-d-13-00082.1
Zhang, X., & Clarke, A. J. (2017). On the dynamical relationship between equatorial Pacific surface currents, zonally averaged equatorial sea level, and El Niño prediction. *Journal of Physical Oceanography*, *47*, 323–337. https://doi.org/10.1175/JPO-D-16-0193.1
Zhao, Y., & Di Lorenzo, E. (2020). The impacts of extra-tropical ENSO precursors on tropical pacific decadal-scale variability. *Scientific Reports*, *10*(1), 12. https://doi.org/10.1038/s41598-020-59253-3
Zhao, Y., Newman, M., Capotondi, A., Di Lorenzo, E., & Sun, D. (2021). Removing the effects of tropical dynamics from North Pacific climate variability. *Journal of Climate*, *34*(23), 9249–9265. https://doi.org/10.1175/jcli-d-21-0344.1
Zhu, J., Huang, B., Cash, B., Kinter, J. L., Manganello, J., Barimalala, R., et al. (2015). ENSO prediction in project minerva: Sensitivity to atmospheric horizontal resolution and ensemble size. *Journal of Climate*, *28*, 2080–2095. https://doi.org/10.1175/jcli-d-14-00302.1